

American Society of Hematology

## Nanoromidepsin, a Polymer Nanoparticle of the HDAC Inhibitor, Improves Safety and Efficacy in Models of T-cell Lymphoma

Tracking no: BLD-2024-027997R2

Ipsita Pal (University of Virginia, United States) Anuradha Illendula (University of Virginia, United States) Andrea Joyner (University of Virginia, United States) John Manavalan (University of Virginia, United States) Tess Deddens (University of Virginia, United States) Ariana Sabzevari (UVA, United States) Deepthi Damera (University of Virginia, United States) Samir Zuberi (University of Virginia, United States) Enrica Marchi (University of Virginia Cancer Center, United States) Todd Fox (University of Virginia, United States) Marya Brown (University of Virginia, United States) Kallesh Danappa Jayappa (University of Virginia, United States) Jihane Khalife (University of Virginia, United States) Jeffrey Craig (University of Virginia Health System, United States) Thomas Loughran (University of Virginia, United States) David Feith (University of Virginia, United States) Owen O'Connor (University of Virginia Cancer Center, United States)

#### Abstract:

Histone deacetylase inhibitors (HDACi) are valued treatment options for patients with T-cell malignancies. Romidepsin is a selective Class I HDACi initially approved for patients with relapsed or refractory (R/R) CTCL and PTCL. Romidepsin was withdrawn from its PTCL indication following a negative randomized Phase IV study (Ro-CHOP) that showed no benefit over CHOP alone, further diminishing options for patients. Herein, we describe the development of a first-in-class polymer nanoparticle (PNP) of romidepsin using an innovative amphiphilic di-block copolymer-based nanochemistry platform. Nanoromidepsin exhibited superior pharmacologic properties with improved tolerability and safety in murine models of T-cell lymphoma (TCL). The PNP also exhibited superior anti-tumor efficacy in multiple models including in vitro -TCL cell lines, ex vivo LGL leukemia patient samples, and murine TCL xenografts. Nanoromidepsin demonstrated greater accumulation in tumors and a statistically significant improvement in overall survival compared to romidepsin in murine xenograft models. These findings justify the clinical development of Nanoromidepsin in patients with T-cell malignancies.

Conflict of interest: COI declared - see note

COI notes: OAO has received consulting fees and/or stock options from Myeloid Therapeutics and Dren Bio as a member of their Scientific Advisory Board, and research support for clinical trial from BMS. DJF has received research funding, honoraria, and/or stock options from AstraZeneca, Dren Bio, Recludix Pharma, and Kymera Therapeutics. TPL has received consultancy fees, honoraria, and/or stock options from Keystone Nano, Flagship Labs 86, Dren Bio, Recludix Pharma, Kymera Therapeutics, and Prime Genomics. JWC has received honoraria from BeiGene and consultancy fees and expert testimony from Bayer. EM reports research funding from Merck, Celgene/Bristol Myers Squibb, Astex Pharmaceuticals, and Myeloid Therapeutics and serves on the data safety monitoring committee with Everest Clinical Research. Other authors declare no competing interests. The funders had no role in the design of the study; in the collection, analyses, or interpretation of data; in the writing of the manuscript; or in the decision to publish the results. A patent has been filed (TREATMENT OF CANCER AND AUTOIMMUNE DISORDERS USING NANO POLYMERS OF HISTONE DEACETYLASE INHIBITORS Application Publication/Patent Number: W02023064634A1, Publication Date: 2023-04-20).

Preprint server: Yes; bioRxiv https://doi.org/10.1101/2024.07.18.603379

Author contributions and disclosures: Conceptualization: IP, AI, TPL, DJF, OAO Methodology: IP, AI, MDB, AJ, JSM, TMD, EM, AS, DPD, SZ, TEF, KDJ, OAO Investigation: IP, AI, JWC, TEF, OAO Visualization: IP, JWC Funding acquisition: TPL, OAO Project administration: IP, OAO Supervision: DJF, OAO Writing - original draft: IP, AI, OAO Writing - review & editing: IP, AI, DPD, SZ, JWC, DJF, KDJ, OAO

Non-author contributions and disclosures: No;

Agreement to Share Publication-Related Data and Data Sharing Statement: For original data, please contact the corresponding author owenaoconnor27@gmail.com

Clinical trial registration information (if any):

# Nanoromidepsin, a Polymer Nanoparticle of the HDAC Inhibitor, Improves Safety and Efficacy in Models of T-cell Lymphoma

Ipsita Pal<sup>1,2,3</sup>, Anuradha Illendula<sup>1,2,3</sup>, Andrea Joyner<sup>1,2,3</sup>, John Sanil Manavalan<sup>1,2</sup>, Tess M. Deddens<sup>1,2,3</sup>, Ariana Sabzevari<sup>1,2,3</sup>, Deepthi P. Damera<sup>1,2,3</sup>, Samir Zuberi<sup>1,2,3</sup>, Enrica Marchi<sup>1,2,3</sup>, Todd E. Fox<sup>2,4</sup>, Marya E. Dunlap-Brown<sup>5</sup>, Kallesh D. Jayappa<sup>1,2,3</sup>, Jihane Khalife<sup>1,2,3</sup>, Jeffrey W. Craig<sup>6</sup>, Thomas P. Loughran Jr. <sup>1,2,3</sup>, David J. Feith<sup>1,2,3</sup>, Owen A. O'Connor<sup>1,2,3,7\*</sup>

<sup>1</sup>University of Virginia Comprehensive Cancer Center, University of Virginia, Charlottesville, VA.

- <sup>2</sup> Division of Hematology and Oncology, University of Virginia; Charlottesville, VA.
- <sup>3</sup> Translational Orphan Blood Cancer Research Center, University of Virginia; Charlottesville, VA.
- <sup>4</sup> Department of Pharmacology, University of Virginia; Charlottesville, VA.
- <sup>5</sup> Molecular Immunologic and Translational Sciences Core, University of Virginia, Charlottesville, VA.
- <sup>6</sup> Department of Pathology, University of Virginia; Charlottesville, VA.
- <sup>7</sup> Department of Microbiology, Immunology and Cancer Biology, University of Virginia; Charlottesville, VA.

Running Title: Nanoromidepsin inhibits T cell malignancies

\*Corresponding author: Owen A. O'Connor.

Mailing address: University of Virginia Comprehensive Cancer Center, Charlottesville, VA, 22903

Email: owenaoconnor27@gmail.com

**Data and materials availability:** All data needed to evaluate the conclusions in the paper are present in the paper and/or the Supplementary Materials.

# **KEY POINTS**

The treatment options for patients with relapsed or refractory PTCL are dwindling, given the paucity of drugs available for these patients.

Leveraging a novel polymer nanochemistry platform we synthesized a new epigenetic modulator with superior features in T-Cell malignancies.

### **ABSTRACT**

Histone deacetylase inhibitors (HDACi) are valued treatment options for patients with T-cell malignancies. Romidepsin is a selective Class I HDACi initially approved for patients with relapsed or refractory (R/R) CTCL and PTCL. Romidepsin was withdrawn from its PTCL indication following a negative randomized Phase IV study (Ro-CHOP) that showed no benefit over CHOP alone, further diminishing options for patients. Herein, we describe the development of a first-inclass polymer nanoparticle (PNP) of romidepsin using an innovative amphiphilic di-block copolymer-based nanochemistry platform. Nanoromidepsin exhibited superior pharmacologic properties with improved tolerability and safety in murine models of T-cell lymphoma (TCL). The PNP also exhibited superior anti-tumor efficacy in multiple models including *in vitro* -TCL cell lines, ex vivo LGL leukemia patient samples, and murine TCL xenografts. Nanoromidepsin demonstrated greater accumulation in tumors and a statistically significant improvement in overall survival compared to romidepsin in murine xenograft models. These findings justify the clinical development of Nanoromidepsin in patients with T-cell malignancies.

### INTRODUCTION

The histone deacetylase inhibitors (HDACi) are important drugs for the treatment of T-cell lymphoma (TCL). Four HDACi have been approved globally for patients with relapsed/refractory (R/R) cutaneous (CTCL) and peripheral T-cell lymphomas (PTCL). While HDACi induce cytotoxicity across many types of malignant disease, clinically their benefits have been confined to patients with TCL. HDACs catalyze the deacetylation of histone and non-histone proteins. Deacetylation of histone leads to the condensation of chromatin (heterochromatin) and transcriptional repression<sup>1</sup>. HDACi prevent deacetylation of histones like histone-3(H3) and histone-4(H4), promoting open chromatin (euchromatin) and transcriptional activation.

There are 11 isoforms of HDAC, classified as I, IIA, IIB, III and IV. Class III HDACs are not affected by any of the available HDACi and are referred to as sirtuins (Sirt), which are known to deacetylate p53. Romidepsin exhibits nanomolar potency against class I HDACs, while most other HDACi would be considered pan-HDACi <sup>2</sup>. While the dissociation constant (Kd) of any HDACi against a particular isoform may vary, it is clear that the profiles of genes activated or repressed by the different HDACi can vary significantly as a function of the HDACi, its concentration, its duration of exposure and the disease specific context. Efforts to ascribe inhibition of a particular HDAC isoform to clinical outcomes have been largely unsuccessful. As a result, these drugs are often considered pleiotropic as they induce a broad spectrum of cellular effects. Complicating this pharmacology is the recognition that HDACs can also deacetylate a host of non-histone proteins like Bcl-6 <sup>3</sup>. The implications of these effects in any given disease are presently unclear.

Despite the reproducible activity of these drugs in patients with R/R PTCL, a recent Phase III trial of Romidepsin-CHOP versus CHOP reported no difference in progression free survival (PFS) or overall survival (OS) between the arms, resulting in withdrawal of the PTCL indication <sup>4</sup>. This, coupled with the recognition that other drugs for R/R PTCL are in regulatory jeopardy, has created legitimate concerns over future management options.

Nanoparticle-based drug design offers the prospect of improved pharmacologic properties, tumor penetration, and intertumoral drug retention with reduced degradation and toxicities <sup>5</sup>. In particular, the development of amphiphilic block co-polymer nanoparticles (PNP) has expanded the repertoire of drugs that can leverage the advantages of nanotherapeutics<sup>6</sup>. We sought to overcome historic liabilities associated with romidepsin, while capitalizing on the benefits of a novel nanochemistry platform. Herein, we report the development of the first polymer

nanoparticle (PNP) of romidepsin and demonstrate the superior safety, targeted delivery and efficacy of the PNP.

### **MATERIALS AND METHODS**

### **Fabrication of Nanoromidepsin**

We adopted a tandem parallel synthesis to achieve optimal Nanoromidepsin physicochemical properties (>500 µg/mL romidepsin, <100 nm particle size, and <0.2 polydispersity index (PDI)) using a versatile nanoprecipitation method. We explored the influence of selected parameters of the nanoprecipitation method including solvent to anti-solvent ratio and drug to polymer ratio to produce romidepsin loaded nanoparticles meeting the pre-determined criteria. For biodistribution studies we co-loaded Nanoromidepsin and the fluorescent tracer DiO into polymer nanoparticles as described above. (See supplemental section for detail).

### Single and Multiple Dose In Vivo Toxicity Study

For single-dose maximum tolerated dose (MTD) studies, BALB/c mice (n=5) received Nanoromidepsin or romidepsin via a single intraperitoneal (IP) or intravenous (IV) dose (1–10 mg/kg), with 14-day monitoring. For repeat-dose studies, NSG mice engrafted with a TCL cell line expressing dTomato and luciferase (H9-dTomato-Luc) cells were treated with ghost PNP, romidepsin, or Nanoromidepsin using various IV dosing regimens (Supplementary methods). Toxicity was assessed by tracking weight loss and clinical scores over time.

### **Pharmacokinetic Study**

Five-to seven-week-old female BALB/c mice were treated with IV or IP Nanoromidepsin or romidepsin. Animals (n=21) received a single dose of one-half MTD as defined by the single dose toxicity study (2.5 mg/kg body weight) of Nanoromidepsin or romidepsin. Mice were sacrificed (n=3 per time point) at 1, 3, 6, 18, 24, 48, and 72 hours after the treatment. Collection of plasma and quantification of romidepsin is described in the Supplementary methods.

### **Biodistribution Study**

Biodistribution of Nanoromidepsin was evaluated in H9-dtomato-luc xenograft. Tumor-bearing NSG mice were randomly assigned into two groups (n = 3) and injected intravenously with Nanoromidepsin co-loaded with DiO or free DiO at an equivalent dose (3.7 mg/kg). Whole-body fluorescence imaging was performed on a cryogenically cooled Lago X (Spectral Instruments Imaging system). Three mice from each group were killed after 72 hours. Tumors and vital organs were harvested for *ex vivo* imaging.

### **Survival and Efficacy Study**

H9-dTomato-luc engrafted mice were randomized to four treatment groups of 9 mice each: (i) PBS control; (ii) ghost PNP; (iii) romidepsin (3.5 mg/kg), or (iv) Nanoromidepsin (3.5 mg/kg) after the minimum tumor luminescence reached 10e6 bioluminescence imaging intensity (BLI; p/s/cm2/sr). All drugs were administered by tail vein once a week. Baseline BLI was completed for all mice the day before the first treatment. *In vivo* BLI analysis was conducted on Lago X (Spectral Instruments Imaging system). A second efficacy/survival study was performed using similar methods with groups with 4 mg/kg (n=9)

## **Statistical Analysis**

Results are presented as the mean ± SD, unless indicated otherwise. Statistical significance was determined by 1-way ANOVA or 2-tailed Student's t test or log-rank test, unless specified otherwise, using GraphPad Prism software, and a p-value of less than 0.05 was considered statistically significant.

#### **RESULTS**

### **Engineering of Nanoromidepsin Loaded PNP**

Different PNPs of romidepsin were synthesized using generally regarded as safe (GRAS) amphiphilic di-block copolymers or FDA-approved lipids for liposomes. Liposomes did not achieve romidepsin encapsulation and were not pursued further. PNPs were synthesized using mPEG-PDLLA and mPEG-PLGA and the surfactant poloxamer-188 using a solvent displacement or nanoprecipitation technique. LC/MS confirmed an average romidepsin concentration in optimized polymer nanoparticles of >500 µg/mL (Figure 1A). mPEG-PDLLA nanoparticles exhibited higher drug concentrations (~540 µg/mL) with an average drug encapsulation efficiency (EE) of 48%. Cryo-EM revealed that both ghost and romidepsin-loaded PNPs exhibited uniform spherical morphology and homogeneous size with no agglomeration (Figure 1B). Dynamic Light Scattering (DLS) revealed a unimodal distribution of particles with an average size of 46.25 nm and a Poly Dispersity Index (PDI) of 0.145 (Figure 1C-D).

The concentration-response relationship for each PNP was compared to romidepsin across a panel of TCL lines and a reference solid tumor cell line (Figures 1E). All three PNPs of romidepsin reduced cell viability in a concentration dependent manner (Figure 1E), though the  $IC_{50}$  values for different PNPs varied across lines (Figure 1F). At 60 hours, most cell lines were consistently sensitive to Nanoromidepsin mPEG-PDLLA H<sub>2</sub>O ( $IC_{50}$ = 0.7-1.9 nM) which was similar to romidepsin ( $IC_{50}$  =0.6-1.9 nM) (Figure 1F). Both Nanoromidepsin mPEG-PDLLA PBS ( $IC_{50}$ =

1.3-7.5 nM) and Nanoromidepsin mPEG-PLGA H<sub>2</sub>O (IC<sub>50</sub>=1.1-5.5) were slightly less potent. There was no growth inhibition of any cell line with the corresponding ghost PNP lacking romidepsin (Figure S1). We employed flow cytometry to identify early chromatin remodeling events and apoptosis, and western blotting to assess later-stage pathway alterations. Flow cytometry and western blotting demonstrated that treatment with all three romidepsin PNPs induced apoptosis similar to romidepsin as shown by increased levels of cleaved PARP (Figure 1H and 1I).

A concentration dependent increase in H3/H4-acetylation was observed by flow cytometry with romidepsin or one of the three romidepsin PNPs (Figure 1G). Among the three PNPs, the Nanoromidepsin mPEG-PDLLA H<sub>2</sub>O PNP was comparable to romidepsin in its pattern of histone acetylation. Western blot analysis demonstrated increased H3/H4 acetylation following exposure to romidepsin or Nanoromidepsin mPEG-PDLLA H<sub>2</sub>O at 24 hours (Figure 1I and 1J). Acetylation of H3 and H4 were 4-fold and 1.5-fold higher in cells treated with 30nM Nanoromidepsin compared to romidepsin (24 hrs).

Between Nanoromidepsin mPEG-PLGA and mPEG-PDLLA, Nanoromidepsin mPEG-PDLLA exhibited superior physicochemical properties (size, PDI and encapsulation efficiency), the lowest IC50 and comparable histone acetylation and PARP cleavage compared to romidepsin, (Figure 1E-1J)). This prompted further optimization, scale up, physicochemical characterization and interrogation of its *in vitro* activity (Figure S2A-2C, S2E-2G)).

### Nanoromidepsin Exhibited Superior Cytotoxicity Against Primary LGL Leukemia Samples

Although romidepsin has not been clinically used in LGL leukemia, this disease model serves to explore Nanoromidepsin's effects across T-cell malignancies. Romidepsin and Nanoromidepsin were compared using LGL-leukemia patient samples. Nanoromidepsin demonstrated superior cytotoxicity in TL-1 (a T-cell LGL) and NKL (a NK-cell LGL) cell lines (Figure S3E). An *ex vivo* cytotoxicity assay performed on PBMC from LGL leukemia patients demonstrated that Nanoromidepsin exhibited a statistically greater potency, (IC $_{50}$ : 3.1 ± 1.7 nM versus IC $_{50}$ : 9.06 ±5.7 nM; p=0.0057) (Figure 2A and 2B). As whole PBMC samples also contain a small proportion of non-leukemic cells, we designed a multi-color flow cytometry-based functional assay<sup>7</sup> to quantify apoptosis in CD3+CD8+CD57+ or CD3+CD8+CD57- cell populations (CD8+ T cell markers) of LGL leukemia patients (Figure 2C). The percentage of CD3+CD8+CD57- and CD3+CD8+CD57+ cells positive for cleaved PARP was similar for Nanoromidepsin and romidepsin treated PBMC samples, though the percentage of dead cells (viability dye+) in CD3+CD8+CD57+ and CD3+CD8+CD57- populations was quantitatively higher

in the Nanoromidepsin treated samples but not statistically significant (p=0.59 and 0.46 respectively) (Figure 2D and 2E).

# Nanoromidepsin Demonstrates Superior Pharmacokinetic Parameters and Biodistribution Compared to Romidepsin

The pharmacokinetic profile of Nanoromidepsin and romidepsin were compared in BALB/c mice by quantifying plasma romidepsin concentrations following IV or IP administration. Irrespective of the route of administration, the plasma concentration of free romidepsin rapidly declined after 6 hours (Figure 3A). Nanoromidepsin exhibited a higher area under the curve (AUC) of exposure 48 hours post-treatment, irrespective of the route of administration. After IV administration, the peak concentration ( $C_{max}$ ), half-life, and AUC for Nanoromidepsin were 10, 1.5, and 25-fold higher compared to free romidepsin respectively (Table 1). The pharmacokinetic (PK) analyses suggested that the clearance of romidepsin was faster following IV compared to IP administration. The peak concentrations achieved after IP administration of Nanoromidepsin and romidepsin were 804 nM and 218 nM, respectively. After IV administration, the peak concentration of Nanoromidepsin and romidepsin were 425 nM and 38 nM, respectively. Based on the *in vitro* data across the TCL cell lines studied, the IC<sub>50</sub> of Nanoromidepsin PDLLA was around 2 to 8 nM (Figure S2F). Collectively, these data suggest that Nanoromidepsin achieves a concentration 50-400-fold greater than the IC<sub>50</sub> of romidepsin with a dose that was only one-half of the MTD of Nanoromidepsin (Figure 3A).

To characterize the biodistribution of Nanoromidepsin, time-dependent tissue and tumor uptake studies were performed. H9-dTomato-luc xenograft mice were administered with Nanoromidepsin co-encapsulated with DiO (Figure S2D). Whole-body florescence imaging demonstrated that the fluorescence signal of Nanoromidepsin-DiO treated mice was greater compared to the free DiO treated mice (Figures 3B and 3C). *Ex vivo* imaging of the organs showed that Nanoromidepsin selectively accumulated in the tumor at 72 hours post-administration. Modest uptake was observed in the liver only in free DiO treated mice. (Figure 3D). Quantification of fluorescent signal in harvested organs showed a significant (p<0.05) accumulation of Nanoromidepsin-DiO in the tumor compared to the free DiO (Figure 3E). In a complementary assay, H9-dTomato-luc engrafted mice were injected with 4 mg/kg romidepsin or Nanoromidepsin. Quantitation of romidepsin in the tumor at 24 hours post-administration revealed an intratumoral concentration of romidepsin in the romidepsin and Nanoromidepsin treated groups of 3.57 and 45.8 ng/mg of protein, respectively. These data demonstrate a substantially greater accumulation of the romidepsin in tumor tissue of Nanoromidepsin treated animals. (Figure 3F). Increased

accumulation was observed in the liver, spleen, and lungs following Nanoromidepsin administration, consistent with clearance via the mononuclear phagocyte system, with no drug detected in the heart. Importantly, no evidence of organ-specific toxicity was observed (Figure S7).

### Nanoromidepsin Exhibits Superior Tolerability Compared to Romidepsin In Vivo

The safety and tolerability of Nanoromidepsin was determined in a single dose toxicity study with escalating doses of Nanoromidepsin or romidepsin (IP and IV) to identify the MTD in BALB/c mice. Changes in body weight and clinical score were assessed as a function of time and dose. While mice in both treatment cohorts experienced weight loss post-treatment, body weight returned to pre-treatment levels in most animals after 15 days (Figures 4A-4B and S3). Mice treated with 8 mg/kg IP of either romidepsin or Nanoromidepsin met criteria for euthanasia three days post-treatment. At this level, 80% of the mice treated with romidepsin were dead 3-days post-treatment, compared to 40% with Nanoromidepsin. This established the MTD for both drugs by IP (5 mg/kg). In the IV cohorts, 10 mg/kg was the highest dose explored for both drugs. Mice lost approximately 15% body weight within three days after treatment with either drug, although all mice in both treatment groups recovered after 15 days. Escalation beyond 10 mg/kg was technically not feasible given the volume of the intravenous dose required at the available Nanoromidepsin concentration.

Although the AUC and C<sub>max</sub> of Nanoromidepsin were considerably higher when drug was administered IP versus IV (Figure 3A), a study in H9-dtomato-luc xenograft confirmed that the IP administration route for Nanoromidepsin induced unacceptably high toxicity (Figure S4). These findings were consistent with the literature suggesting that many nanoparticles cannot be administered safely by the IP route given the association with peritonitis likely due to the physical features of the particle <sup>8</sup>. For these reasons, all subsequent *in vivo* studies used only the IV route.

Multi-dose studies were conducted in H9-dTomato-luc xenograft-containing NSG mice (Table S1, and Figures S5 and S6). approximating the single agent dose-intensity and corresponding to ¼, ½, and ¾ of the MTD for Nanoromidepsin. Repeat dosing studies revealed that romidepsin produced a higher degree of weight loss (>10%) and clinical score (>3) compared to Nanoromidepsin at equivalent dose. The most tolerated dose and schedule of Nanoromidepsin was identified to be 4 mg/kg once weekly for three weeks (Figure 4C-D). Romidepsin at a dose of 8 mg/kg demonstrated acute toxicity leading to death of all mice (thus LD50 is significantly less than 8 mg/kg) within four days, while 8 mg/kg Nanoromidepsin was lethal in only 50% of mice, representing the LD50 of Nanoromidepsin (Figures 4E and 4F).

To assess tissue-specific toxicity, liver and tumor were assessed for histopathology. (Figure 4G). Liver sections from all cohorts exhibited normal microarchitecture without any indication of inflammation or necrosis. Although there were no signs of drug induced toxicity in the liver sections of either treatment cohort, the LC-MS quantification confirmed that the concentrations of romidepsin in the liver were substantially less with Nanoromidepsin compared to romidepsin (13.18 and 46.68 ng/mg of protein, respectively (p<0.0009) (Figure 4H). Tumor sections from the mice treated with the ghost PNP revealed sheet-like infiltrates of large, atypical lymphocytes with pleomorphic nuclei, distinct nucleoli and amphophilic cytoplasm, consistent with viable tumor. The romidepsin and Nanoromidepsin-treated tumor sections showed varying degrees of treatment-related necrosis, with no substantial difference in histopathology between the treatment groups. The mean plasma concentrations of romidepsin at 1 and 24 hours following three consecutive treatments of romidepsin (weekly doses for three weeks) were 51 and 4.9 ng/mL (Figure 4I). These data indicate a rapid decline in mean plasma concentration, implying a rapid clearance of romidepsin from the blood. In contrast, the mean plasma concentrations of romidepsin in the plasma collected at 1 and 24 hours following the same dose of Nanoromidepsin were 120.3 and 40.7 ng/mL, (2.3 and 8.3-fold greater than the free romidepsin).

# Nanoromidepsin Shows Superior Activity and a Survival Advantage in Murine Xenograft Models

To determine differences in efficacy, H9-dmotato xenograft engrafted mice were treated with 3.5 mg/kg weekly for 3 weeks with romidepsin or Nanoromidepsin (Figure 5A). After three treatments, the cohort receiving romidepsin exhibited moderate anti-tumor activity with tumor growth inhibition assessed by BLI of 54% and 57% compared to the vehicle and ghost PNP cohorts, respectively (p=0.0315 vs vehicle; p=0.04 vs ghost PNP). Nanoromidepsin inhibited tumor growth by 90% and 91% compared to the vehicle and ghost PNP cohorts respectively (p=0.0003 vs vehicle; p=0.0019 vs ghost PNP). While there was no statistically significant difference in the growth delay observed between romidepsin and Nanoromidepsin (p=0.6665), the Nanoromidepsin cohort demonstrated greater tumor reduction by BLI compared to romidepsin after 3 weeks of treatment (Figure 5B). The tumor BLI signal was reduced one week after the first treatment which held constant for the next three weeks for both treatment cohorts (Figure 5B, 5D, and 5E) supporting Nanoromidepsin's superiority. Mice treated with Nanoromidepsin or romidepsin showed no statistically significant survival benefit at this dose which may be due to cytokinetic failures resulting from compromised dose intensity (Figure 5C).

In response to the insignificant survival benefit as observed in Figure 5 likely due to the low dose and short treatment time, we administered both drugs at on a 35 days cycle at 4 mg/kg/week for four-consecutive weeks, (Figure 6A). Significant toxicity was noted after one cycle with romidepsin. A consistent increase in the BLI was observed in the PBS, ghost PNP and romidepsin treated mice cohort until day 24 (Figures 6B and 6C). A growth delay was observed in the Nanoromidepsin cohort. Moreover, 33% of mice died after three weeks of treatment with romidepsin, while treatment with Nanoromidepsin resulted in no deaths (Figure 6C). Nanoromidepsin resulted in a statistically significant prolongation in OS compared to romidepsin (Figure 6D). The overall survival in the control, ghost PNP and romidepsin treated mice was 38 days (for all three groups), compared to 53 days with Nanoromidepsin (p<0.001). We did observe some toxicity after third treatment in Cycle 2, suggesting that perhaps a lower maintenance dose might be worth exploring in the future. These data demonstrate superior biological activity, efficacy, and survival benefit of Nanoromidepsin compared to romidepsin.

### **DISCUSSION**

The dwindling options to treat patients with R/R PTCL has created an urgent need to rethink how we develop new drugs for challenging orphan diseases. In the U.S., pralatrexate and belinostat are the only drugs still approved for patients with R/R PTCL, albeit they are not full approvals. Loss of the romidepsin indication in R/R PTCL has put physicians and patients in a challenging position. With few new drugs emerging, improving existing treatments or developing new ones through combinatorial regimens offers a relatively low-risk way to advance care.

Romidepsin in combination with other epigenetically targeted drugs like the DNMT inhibitor 5-azacytidine appears to produce the best overall response rate (ORR) and PFS data of any drug or drug combination to date in this population <sup>9,10</sup>. These clinical and preclinical experiences suggest that combinations with an HDACi, romidepsin being among the most potent, may represent one straight-forward path to create new treatment platforms for this population<sup>11,12</sup>. While preclinical data highlight romidepsin's superior potency compared to other HDAC inhibitors clinically, romidepsin produces an ORR of 25%, a PFS of 3-4 months, and a median response duration exceeding a year, all disappointing results given the preclinical findings. This discrepancy may stem from its suboptimal pharmacologic properties, including high protein binding (92%-94%), a short half-life (3.8 hours), and limited volume of distribution (Vd) (44.5L), which constrain its effects on transcriptional activation <sup>13,14</sup>.

Pharmacologic optimization offers a path to overcome the intrinsic limitations of therapeutic agents, and PNPs offer the prospect of resolving the liabilities associated with sub-

optimized drugs 15. The amphiphilic diblock lactides used to make PNP are considered biocompatible, biodegradable and non-toxic, which enhances their elimination, improves their tolerability, and reduces their immunogenicity <sup>16</sup>. The inclusion of the PEG chain to the PNP has been shown to reduce the elimination of the particles via the host immune system, maximizing circulation time <sup>17</sup>. An attractive feature of this platform is that hydrophobic drugs can be readily incorporated and even conjugated to the polymer <sup>18-20</sup>. In our case, PEGylation likely protects romidepsin by forming a hydrophilic barrier that blocks external reducing agents like glutathione and serum thiols, stabilizing romidepsin's oxidized disulfide state while preventing premature reduction. In addition, PNPs typically have a size of less than 100nm which aids in improving the volume of distribution allowing for a bioconcentration of drug in tissue, particularly tumor. Herein, we exploited the unique physicochemical properties of a tailored PNP, including optimal size and surface properties, enhanced Vd, and augmented tumor bioavailability, in an effort to address the limitations of "naked" romidepsin. The goal was to enhance the epigenetic effects of the drug deploying a scalable translational approach 21-23. We designed our PNP particles to be approximately 50 nm, which has been suggested to be a feature that favors bioconcentration in the tumor microenvironment 24. The bioluminescent in vivo assay which deployed a PNP containing both romidepsin and DiO clearly established a predilection for the PNP to bioaccumulate in the tumor microenvironment. While several mechanisms can explain this, porous and leaky vasculature have been advanced as one of the major explanations <sup>25-30</sup>.

In PTCL patients, administration of romidepsin (14 mg/m² IV over 4-hours on days 1, 8, and 15 of a 28-day cycle yields a C<sub>max</sub> and AUC0-∞ of 377 ng/mL and 1549 ng\*hr/mL, respectively. In rats, single slow IV bolus of romidepsin administration (0.33 and 0.67 mg/kg) achieved a mean AUC∞ of 10.3 and 18.1 ng\*hr/mL, respectively <sup>31</sup>. Following a single IV dose of romidepsin and Nanoromidepsin, the C<sub>max</sub> in BALB/c mice was 21.3 and 231.0 ng/ml respectively. Another major difference was seen in the AUC, which was 99.2 and 2532.1 ng\*hr/mL for romidepsin and Nanoromidepsin, respectively. Nanoromidepsin exhibited a 1.5-fold increase in half-life compared to romidepsin, indicating prolonged availability in plasma. Recognizing all the cross-species differences, these data suggest that Nanoromidepsin in these murine models approximated or dramatically exceeded those PK parameters established in humans which is also supported by our biodistribution study where PNP was shown to preferentially bioaccumulate in tumor. Some conventional polymeric nanoparticles have been shown to accumulate in organs like the spleen, liver, and kidneys, potentially limiting their therapeutic potential <sup>17</sup>. This is important as we observed similar findings after a short-term treatment, though the BLI imaging confirmed selective bioaccumulation of Nanoromidepsin at later time points in tumor. These findings are concordant

with previous studies indicating that a PNP tailored for the Active Pharmaceutical Ingredient can improve bioavailability thereby optimizing mechanism of action <sup>32,33</sup>, a factor that may be especially important for drugs targeting the epigenome.

The improvement in the PK parameters raises concerns about incrementally worse tolerability. In a series of comprehensive single and repeat dose toxicity studies, Nanoromidepsin was found to be substantially safer than romidepsin, even at the highest doses studied. These data have established a sound basis to identify the MTD, optimal route of administration, and acceptable dosing schedule prior to the efficacy studies. Our *in vivo* toxicity assays affirmed that Nanoromidepsin was safer compared to romidepsin and exhibited less accumulation in the liver as shown in biodistribution studies and as supported by the histopathology and LC-MS-based quantification of drug in vital organs. In the xenograft models, Nanoromidepsin exhibited an LD50 value of 8 mg/kg, compared to 5 mg/kg for romidepsin (Figure 4E and S6). The direct comparison of body weight loss and clinical toxicity scores in mice confirmed the superior safety profile of Nanoromidepsin at all doses and schedules studied.

Across all efficacy studies, Nanoromidepsin dosed at 4 mg/kg weekly for 4 consecutive weeks followed by re-treatment produced substantially superior growth delay, and an overall survival advantage compared to romidepsin. An overall survival advantage is based on the depth of a complete remission (CR). In clinical practice, durable remissions are often achieved with multiple cycles of combination therapy. The improved tolerability and efficacy of Nanoromidepsin would suggest that combinations of drugs with Nanoromidepsin will further deepen the CR, likely translating into improved outcomes for patients with PTCL.

In summary, we have pioneered the development of a unique epigenetically targeted PNP, which exhibits superior pharmacokinetic features, tolerability and efficacy compared to the historically approved drug. This study represents the first to interrogate the merits of a PNP platform into the pharmacology of an epigenetically targeted drug for these diseases. Future studies will address the mechanisms that account for the bioaccumulation of the romidepsin PNP in the tumor microenvironment, as well as the differences in gene expression and how this might explain the potent efficacy advantage for Nanoromidepsin. We believe the platform has created an opportunity to reconfigure the traditional treatment paradigms for patients with PTCL, as we now poise this drug for future clinical studies.

Acknowledgments: This manuscript is dedicated to the memory of Dr. Mark Kester, a colleague, friend, and pioneer in the field of nanochemistry. We acknowledge Jeremy Gatesman, Joshua Tennant and Susan Walker for their technical support. We acknowledge Molecular Immunologic & Translational Sciences (MITS) Core for animal work, Metabolomics Core for nanoparticle characterization, and Flow Cytometry Core facilities.

### **Funding:**

OAO is grateful for the American Cancer Society Professorship.

OAO is funded in part by Grant 1R01FD006814-01.

The LC-MS work is supported by P30 CA044579 (TEF).

The authors are indebted to the Scarlet Feather Foundation support for the TOBCRI and the IVY Foundation for their continued support.

The authors thank University of Virginia LGL Leukemia Registry personnel for their support of this study. The Registry was supported by the Bess Family Charitable fund and a gift from a generous anonymous donor (TPL).

The data for this (manuscript or presentation) were generated in the University of Virginia Flow Cytometry Core Facility (RRid:SCR\_017829) and is partially supported by the NCI Grant (P30-CA044579).

### **Author contributions:**

Conceptualization: IP, AI, TPL, DJF, OAO

Methodology: IP, AI, MDB, AJ, JSM, TMD, EM, AS, DPD, SZ, TEF, KDJ, OAO

Investigation: IP, AI, JWC, TEF, OAO

Visualization: IP, JWC

Funding acquisition: TPL, OAO Project administration: IP, OAO

Supervision: DJF, OAO

Writing – original draft: IP, AI, OAO

Writing - review & editing: IP, AI, DPD, SZ, JWC, DJF, KDJ, OAO

### **Competing interests:**

OAO has received consulting fees and/or stock options from Myeloid Therapeutics and Dren Bio as a member of their Scientific Advisory Board, and research support for a clinical trial from BMS. DJF has received research funding, honoraria, and/or stock options from AstraZeneca, Dren Bio, Recludix Pharma, and Kymera Therapeutics. TPL has received consultancy fees, honoraria,

and/or stock options from Keystone Nano, Flagship Labs 86, Dren Bio, Recludix Pharma, Kymera Therapeutics, and Prime Genomics. JWC has received honoraria from BeiGene and consultancy fees and expert testimony from Bayer. EM reports research funding from Merck, Celgene/BMS, DREN Bio, Kyowa Kirin, Vittoria Biotherapeutics, Acrotech, and Everest Clinical Research. Other authors declare no competing interests. The funders had no role in the design of the study; in the collection, analyses, or interpretation of data; in the writing of the manuscript; or in the decision to publish the results. A patent has been filed (TREATMENT OF CANCER AND AUTOIMMUNE DISORDERS USING NANO POLYMERS OF HISTONE DEACETYLASE INHIBITORS Application Publication/Patent Number: WO2023064634A1, Publication Date: 2023-04-20).

### **REFERENCES**

- 1. Saksouk N, Simboeck E, Dejardin J. Constitutive heterochromatin formation and transcription in mammals. *Epigenetics Chromatin*. 2015;8:3.
- 2. Bradner JE, West N, Grachan ML, et al. Chemical phylogenetics of histone deacetylases. *Nat Chem Biol.* 2010;6(3):238-243.
- 3. Glozak MA, Sengupta N, Zhang X, Seto E. Acetylation and deacetylation of non-histone proteins. *Gene*. 2005;363:15-23.
- 4. Bachy E, Camus V, Thieblemont C, et al. Romidepsin Plus CHOP Versus CHOP in Patients With Previously Untreated Peripheral T-Cell Lymphoma: Results of the Ro-CHOP Phase III Study (Conducted by LYSA). *J Clin Oncol*. 2022;40(3):242-251.
- 5. Yao Y, Zhou Y, Liu L, et al. Nanoparticle-Based Drug Delivery in Cancer Therapy and Its Role in Overcoming Drug Resistance. *Front Mol Biosci.* 2020;7:193.
- 6. Gagliardi A, Giuliano E, Venkateswararao E, et al. Biodegradable Polymeric Nanoparticles for Drug Delivery to Solid Tumors. *Front Pharmacol.* 2021;12:601626.
- 7. Jayappa KD, Gordon VL, Morris CG, et al. Extrinsic interactions in the microenvironment in vivo activate an antiapoptotic multidrug-resistant phenotype in CLL. *Blood Adv.* 2021;5(17):3497-3510.
- 8. Petros RA, DeSimone JM. Strategies in the design of nanoparticles for therapeutic applications. *Nat Rev Drug Discov*. 2010;9(8):615-627.
- 9. Falchi L, Ma H, Klein S, et al. Combined oral 5-azacytidine and romidepsin are highly effective in patients with PTCL: a multicenter phase 2 study. *Blood*. 2021;137(16):2161-2170.
- 10. O'Connor OA, Falchi L, Lue JK, et al. Oral 5-azacytidine and romidepsin exhibit marked activity in patients with PTCL: a multicenter phase 1 study. *Blood*. 2019;134(17):1395-1405.
- 11. Jain S, Jirau-Serrano X, Zullo KM, et al. Preclinical pharmacologic evaluation of pralatrexate and romidepsin confirms potent synergy of the combination in a murine model of human T-cell lymphoma. *Clin Cancer Res.* 2015;21(9):2096-2106.
- 12. Scotto L, Kinahan C, Douglass E, et al. Targeting the T-Cell Lymphoma Epigenome Induces Cell Death, Cancer Testes Antigens, Immune-Modulatory Signaling Pathways. *Molecular Cancer Therapeutics*. 2021;20(8):1422-1430.
- 13. Coiffier B, Pro B, Prince HM, et al. Results from a pivotal, open-label, phase II study of romidepsin in relapsed or refractory peripheral T-cell lymphoma after prior systemic therapy. *J Clin Oncol*. 2012;30(6):631-636.
- 14. Piekarz RL, Frye R, Prince HM, et al. Phase 2 trial of romidepsin in patients with peripheral T-cell lymphoma. *Blood*. 2011;117(22):5827-5834.

- 15. Kamaly N, Xiao Z, Valencia PM, Radovic-Moreno AF, Farokhzad OC. Targeted polymeric therapeutic nanoparticles: design, development and clinical translation. *Chem Soc Rev.* 2012;41(7):2971-3010.
- 16. Ben-Akiva E, Est Witte S, Meyer RA, Rhodes KR, Green JJ. Polymeric micro- and nanoparticles for immune modulation. *Biomater Sci.* 2018;7(1):14-30.
- 17. Cheng CJ, Tietjen GT, Saucier-Sawyer JK, Saltzman WM. A holistic approach to targeting disease with polymeric nanoparticles. *Nat Rev Drug Discov*. 2015;14(4):239-247.
- 18. Ye W, Zhu F, Cai Y, et al. Improved paclitaxel delivery with PEG-b-PLA/zein nanoparticles prepared via flash nanoprecipitation. *Int J Biol Macromol*. 2022;221:486-495.
- 19. Ibrahim AH, Ibrahim HM, Elbahwy IA, Afouna MI, Tagami T, Ozeki T. Lyophilized tablets of felodipine-loaded polymeric nanocapsules to enhance aqueous solubility: Formulation and optimization. *Journal of Drug Delivery Science and Technology*. 2022;70:103172.
- 20. Ji J, Qin H, Yang Y, Wu J, Wu J. The targeting imaging and treatment capacity of gelsolintargeted and paclitaxel-loaded PLGA nanoparticles in vitro and in vivo. *Front Bioeng Biotechnol*. 2022;10:933856.
- 21. Barichello JM, Morishita M, Takayama K, Nagai T. Encapsulation of hydrophilic and lipophilic drugs in PLGA nanoparticles by the nanoprecipitation method. *Drug Dev Ind Pharm*. 1999;25(4):471-476.
- 22. Fessi H, Puisieux F, Devissaguet JP, Ammoury N, Benita S. Nanocapsule formation by interfacial polymer deposition following solvent displacement. *International Journal of Pharmaceutics*. 1989;55:1-4.
- 23. Bhatia SN, Chen X, Dobrovolskaia MA, Lammers T. Cancer nanomedicine. *Nat Rev Cancer*. 2022;22(10):550-556.
- 24. Tang L, Yang X, Yin Q, et al. Investigating the optimal size of anticancer nanomedicine. *Proc Natl Acad Sci U S A*. 2014;111(43):15344-15349.
- 25. Fang J, Nakamura H, Maeda H. The EPR effect: Unique features of tumor blood vessels for drug delivery, factors involved, and limitations and augmentation of the effect. *Adv Drug Deliv Rev.* 2011;63(3):136-151.
- 26. Edlund U, Albertsson A-C. Degradable Polymer Microspheres for Controlled Drug Delivery. Degradable Aliphatic Polyesters. Berlin, Heidelberg: Springer Berlin Heidelberg; 2002:67-112.
- 27. Musumeci T, Ventura CA, Giannone I, et al. PLA/PLGA nanoparticles for sustained release of docetaxel. *Int J Pharm.* 2006;325(1-2):172-179.
- 28. Danhier F, Ansorena E, Silva JM, Coco R, Le Breton A, Préat V. PLGA-based nanoparticles: an overview of biomedical applications. *J Control Release*. 2012;161(2):505-522.
- 29. Demento SL, Eisenbarth SC, Foellmer HG, et al. Inflammasome-activating nanoparticles as modular systems for optimizing vaccine efficacy. *Vaccine*. 2009;27(23):3013-3021.
- 30. Deng WJ, Yang XQ, Liang YJ, et al. FG020326-loaded nanoparticle with PEG and PDLLA improved pharmacodynamics of reversing multidrug resistance in vitro and in vivo. *Acta Pharmacol Sin.* 2007;28(6):913-920.
- 31. Istodax (Report 501650; package insert); Celgene Corporation (Bristol Myers Squibb).
- 32. Mugheirbi NA, Paluch KJ, Tajber L. Heat induced evaporative antisolvent nanoprecipitation (HIEAN) of itraconazole. *Int J Pharm.* 2014;471(1-2):400-411.
- 33. Keck CM, Müller RH. Drug nanocrystals of poorly soluble drugs produced by high pressure homogenisation. *Eur J Pharm Biopharm*. 2006;62(1):3-16.

Table 1: Pharmacokinetic parameters of romidepsin and Nanoromidepsin after IP and IV route of administration

| Route of administration |         | Intraperitoneal    |                    |                            | Intravenous            |                    |                               |
|-------------------------|---------|--------------------|--------------------|----------------------------|------------------------|--------------------|-------------------------------|
| Parameter               | Unit    | Free<br>Romidepsin | Nano<br>Romidepsin | Fold change<br>(Nano/Free) | Free<br>Romide<br>psin | Nano<br>Romidepsin | Fold<br>change<br>(Nano/Free) |
| T1/2                    | h       | 9.8                | 11.6               | 1.2                        | 5.2                    | 7.6                | 1.5                           |
| Tmax                    | h       | 6.0                | 3.00               | 2                          | 1.00                   | 1.00               |                               |
| Cmax                    | ng/ml   | 119.9              | 434.7              | 3.6                        | 21.3                   | 231.0              | 10.8                          |
| AUC 0-t                 | ng/ml*h | 1918.9             | 6939.9             | 3.6                        | 99.2                   | 2532.1             | 25.5                          |

T1/2- Half life; Tmax-time to maximum plasma concentration; Cmax- maximum plasma concentration; AUC 0-t- the area under the curve up to the last quantifiable time-point

### FIGURE LEGENDS

Figure 1. Romidepsin nanoparticle synthesis, physicochemical characterization, and drug activity analysis in PTCL cells in vitro.

(A) Carrier selection screening. Romidepsin encapsulation quantified by LC/MS;

- (B) Cryo-EM of different analogs of Nanoromidepsin to identify the size and morphology of PNPs in synthesized in different solvents. (i) Ghost in H2O (ii) Nanoromidepsin in H2O (iii) Nanoromidepsin in PBS;
- (C) DLS graphs (top) and Zeta-potential (bottom) spectra of Nanoromidepsin in H2O;
- (D) DLS and Zeta potential data of Nanoromidepsin ghost and Nanoromidepsin in H2O;
- **(E)** HH and H9 (CTCL), SUPM2 (ALK+ ALCL) TL-1 (LGL leukemia), NKL (NK-cell lymphoblastic leukemia/lymphoma), FM3-29 (melanoma) were treated with romidepsin and different analogs of Nanoromidepsin (mPEG-PDLLA Nanoromidepsin-H2O, mPEG-PDLLA Nanoromidepsin PBS and mPEG-PLGA Nanoromidepsin H2O) to explore the impact on the cell viability of different Nanoromidepsin analogs manufactured using combinations of different polymers (PDLLA and PLGA) and solvents (PBS and H2O). The cytotoxicity was determined using CellTiter-Glo assay after 60 hours of treatment.
- **(F)** IC50 (nM) for romidepsin and Nanoromidepsin analogs for the six cell lines at 60 hours. Flow cytometry of **(G)** Ac-H3 (Lys27), and Ac-H4 (Lys16) **(H)** cleaved PARP expressing in HH cell line after 30 hours of treatment with indicated treatment of increasing concentration of romidepsin and Nanoromidepsin. Data presented as mean ± SD;
- (I) Western blot analysis of Ac-H3(Lys27), Ac-H4 (Lys16), and cleaved PARP at 24 hours after treatment with Ghost, romidepsin, and Nanoromidepsin mPEG-PDLLA H2O, and (J) densitometry analysis of the Western blot analysis.

# Figure 2. Effect of Nanoromidepsin on Primary LGL Leukemia patient PBMC samples.

- **(A)** Freshly frozen PBMCs from LGL leukemia patients were treated with indicated doses of romidepsin (solid line) or Nanoromidepsin (dotted line) for 48 hours.
- (B) IC50 (nM) for romidepsin and Nanoromidepsin for 10 LGL leukemia patients at 48 hours;
- **(C)** PBMCs from patients with LGL leukemia and healthy donor as a control were screened by flow cytometry. The lymphocyte and singlet cell gating were performed as described earlier. The CD3+/CD8+/CD57+/- cells were gated from singlet lymphocyte population as indicated. The cleaved PARP or viability dye staining was analyzed in CD3+/CD8+/CD57+ or CD3+/CD8+/CD57- cells as indicated. The flow images were generated from a representative LGL patient (PT #03) PBMC sample treated with DMSO or romidepsin (10 nM). Ghost or Nanoromidepsin treated samples were similarly analyzed;
- **(D)** Cleaved PARP (apoptosis) and (E) live-dead dye staining (cell viability) after the incubation with romidepsin and Nanoromidepsin for 48 hours. Data presented as percentage CD3+/CD8+/CD57+ (more differentiated LGL) or CD3+/CD8+/CD57- (less differentiated LGL) cells positive for cleaved PARP or live-dead dye staining. The data presented after subtracting spontaneous apoptosis or cell viability values from the DMSO-treated controls.

### Figure 3. Pharmacokinetics and tissue distribution of Nanoromidepsin in vivo.

- (A) Plasma concentration-time dependence plot of romidepsin concentration in plasma after intraperitoneal or intravenous administration of a single treatment with romidepsin or Nanoromidepsin;
- **(B)** Diagram representing experimental time-points associated with Nanoromidepsin co-loaded with a fluorescent dye DiO or free DiO administration and fluorescent images evaluation, as well as organs collection;

- **(C)** Fluorescence images of H9-dTomato-luc tumor-bearing mice taken at different time points after intravenous injection of free DiO or DiO and romidepsin encapsulated nanoparticle (NanoromiDiO);
- **(D)** Ex vivo fluorescence images and **(E)** corresponding optical intensity of tumor and major organs (tumor, liver, spleen, kidney, heart, and lung, respectively) dissected at 72 h post-injection. Statistical significance was determined by using student t test (Mann-Whitney) where \*, p<0.05, \*\*< p<0.01, \*\*\*, p<0.001;
- **(F)** Mice bearing H9-dtomato-luc xenograft were treated with 4 mg/kg romidepsin and Nanoromidepsin. After 24h, tumors (n=3) were collected for LC-MS based quantification of romidepsin in tumor tissue.

### Figure 4. Tolerability of romidepsin and Nanoromidepsin in vivo.

BALB/c mice were administered a single dose of romidepsin or Nanoromidepsin (A) IP (B) IV. Tolerability was assessed by monitoring body weight and overall health conditions. X represents dead mice:

H9-dTmato-luc xenograft-bearing NSG mice were administered 4 mg/kg of romidepsin or Nanoromidepsin by IV or IP for arrow indicated days (1, 8 and 15 days). (C) Percentage of body weight changes as function of starting weights (+/-SEM) are shown; (D) clinical score. H9-dTmato-luc xenograft-bearing NSG mice administered with 8 mg/kg of romidepsin or Nanoromidepsin by IV for arrow indicated days. Depicted are (E) percentage of body weight changes as function of starting weights (+/-SEM); (F) clinical score;

- **(G)** Liver and tumor were harvested, fixed in formalin for pathological analysis following H&E staining and processed for LC-MS based quantification of romidepsin. H&E staining of hepatic parenchyma from ghost, romidepsin, and Nanoromidepsin treated mice (original magnifications X200). Soft tissue-based tumors from ghost-treated mice with pleomorphic nuclei, and brisk mitosis (original magnification X1000). Romidepsin and Nanoromidepsin-treated tumors associated with varying treatment-related necrosis (original magnifications X1000). Red and black arrows indicate mitotic figures and necrosis/apoptosis; **(H)** LC-MS based quantification from liver;
- (I) Blood was collected by sub-mandibular bleeding after 1 and 24 hours following the last treatment with 4 mg/kg romidepsin and Nanoromidepsin in the repeat dose study. Plasma was collected and the romidepsin was quantified. LC-MS based quantification of plasma collected from 4C after 1 and 24 hours. Statistical significance was determined by using student t-test (Mann-Whitney) where \*, p<0.05, \*\*< p<0.01, \*\*\*, p<0.001.

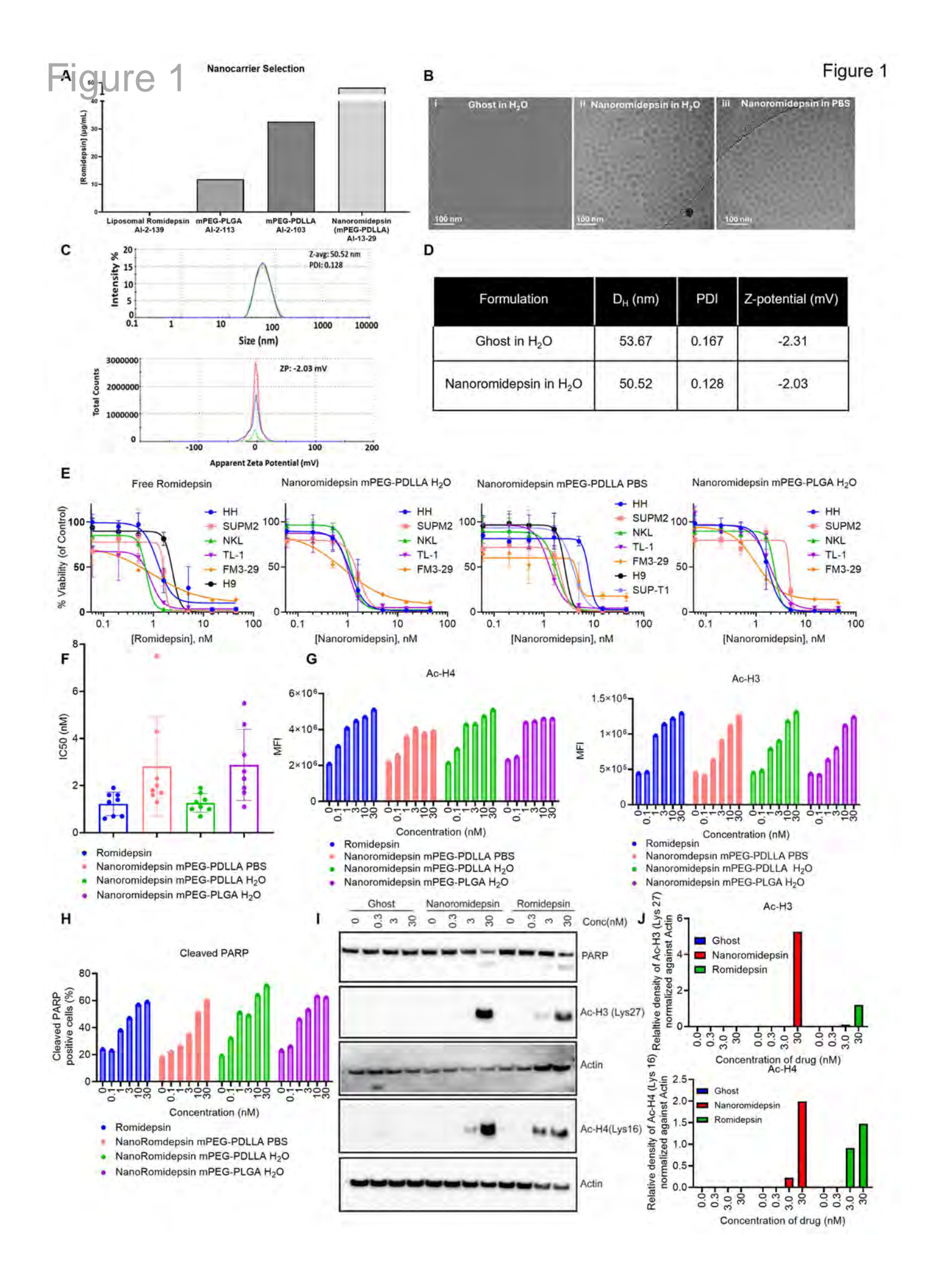
# Figure 5. Nanoromidepsin showed superior activity but similar survival rate compared to romidepsin in TCL xenograft bearing NSG mice.

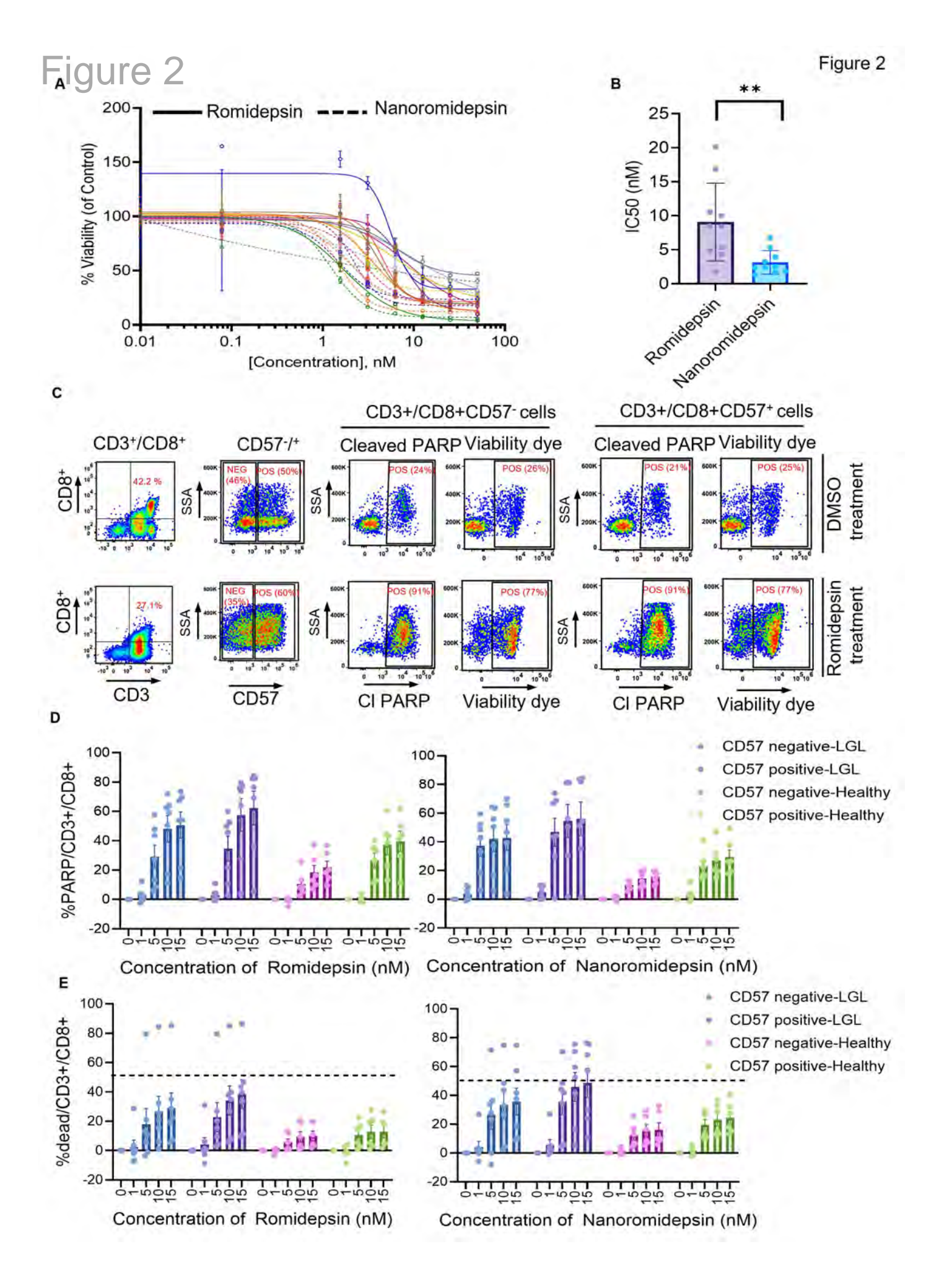
- **(A)** Diagram representing the inoculation and dosing schedule of romidepsin and Nanoromidepsin in H9-dtomato-luc xenograft bearing mice;
- **(B)** and **(D)** Region-of-interest analysis of BLIs (readout for tumor growth) from different treatment groups were recorded at various time points over the course of 8 weeks. Statistical significance was determined by using student t test (Mann-Whitney) where \*, p<0.05, \*\*< p<0.01, \*\*\*, p<0.0001;
- **(C)** Survival curves for romidepsin–treated, Nanoromidepsin-treated, ghost nanoparticle and control mice (n = 9 per group). The arrows indicate treatment days. Statistical significance was determined by using log rank test where \*, p<0.05, \*\*< p<0.01, \*\*\*, p<0.001;

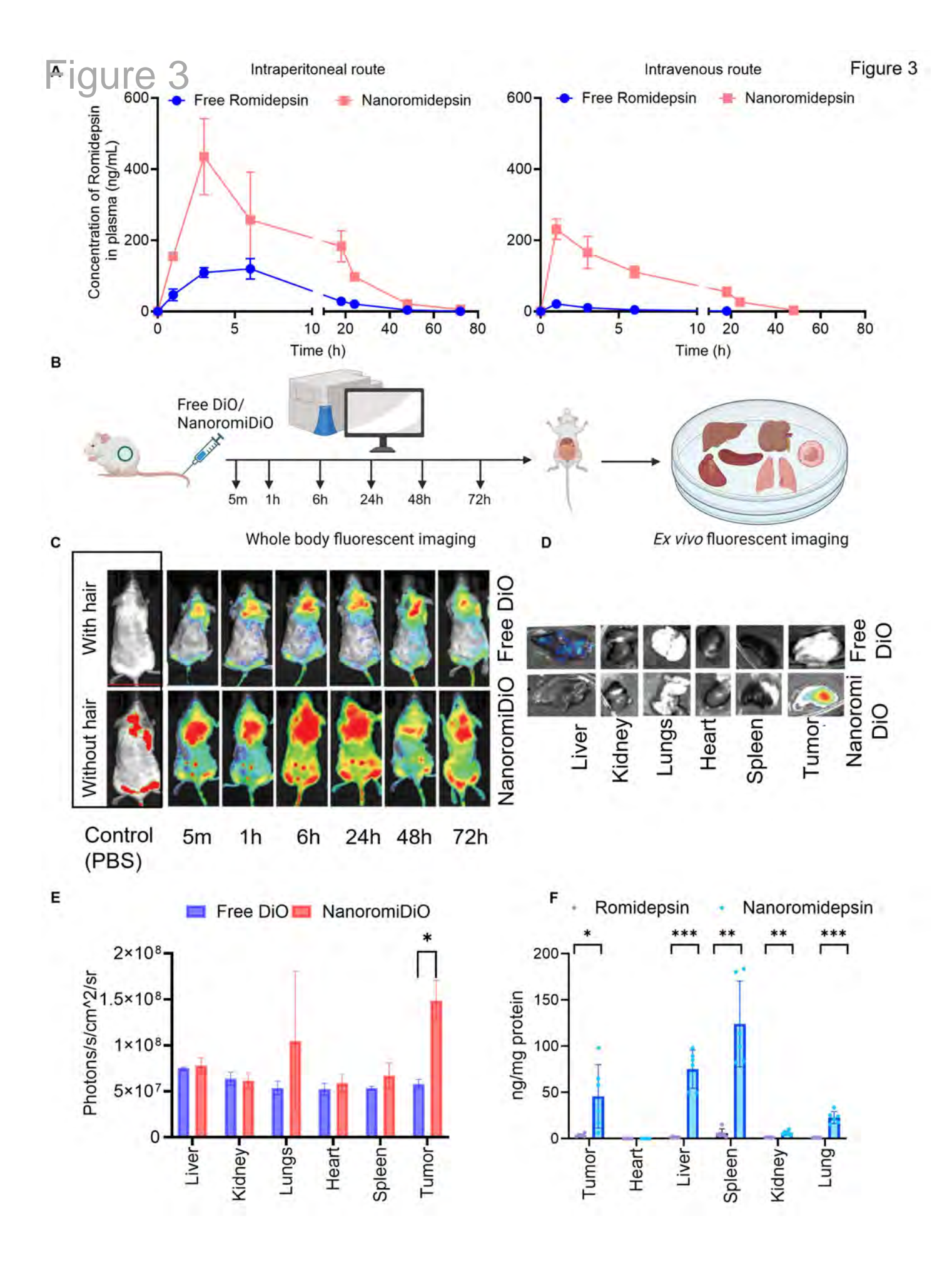
**(E)** Whole-body bioluminescence images of H9-dTomato-luc xenograft–bearing mice taken at the indicated day. Red box indicates dead mouse.

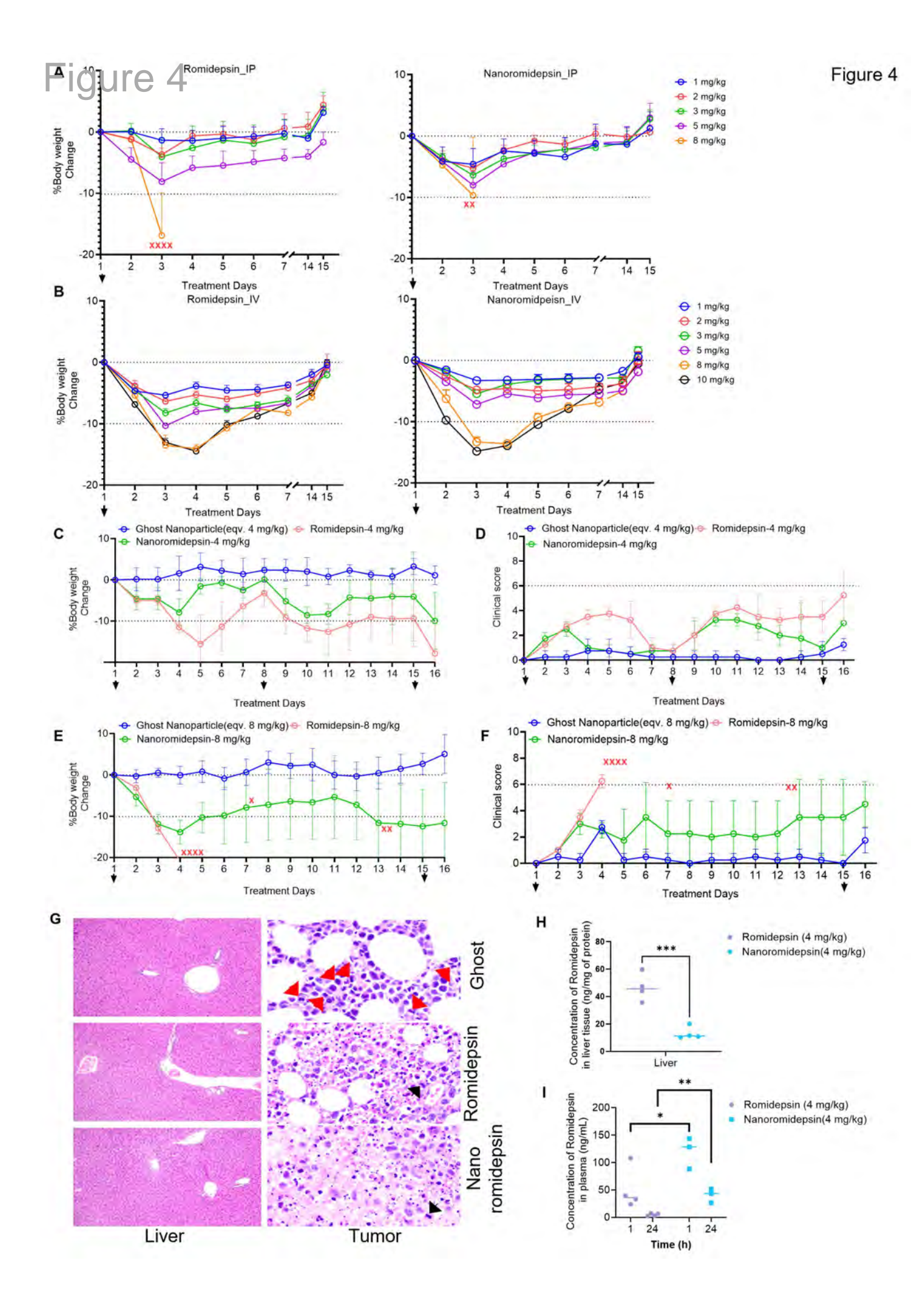
# Figure 6. Dosing schedule change of Romidepsin encapsulated nanoparticle showed superior activity and survival rate compared to romidepsin in CTCL xenograft bearing NSG mice.

- **(A)** Diagram representing the inoculation and dosing schedule of romidepsin and Nanoromidepsin in TCL xenograft bearing mice;
- **(B)** Region-of-interest analysis of BLIs (readout for tumor growth) from different treatment groups at various time points during the course of treatment and plotted as bar graph;
- **(C)** Whole-body bioluminescence images of H9-dTomato-luc xenograft–bearing mice taken at the indicated day;
- **(D)** Survival curves for romidepsin–treated, Nanoromidepsin-treated, ghost nanoparticle and control mice (n = 9 per group). The arrows indicate treatment days. Statistical significance was determined by using log rank test where \*, p<0.05, \*\*< p<0.01, \*\*\*, p<0.001.



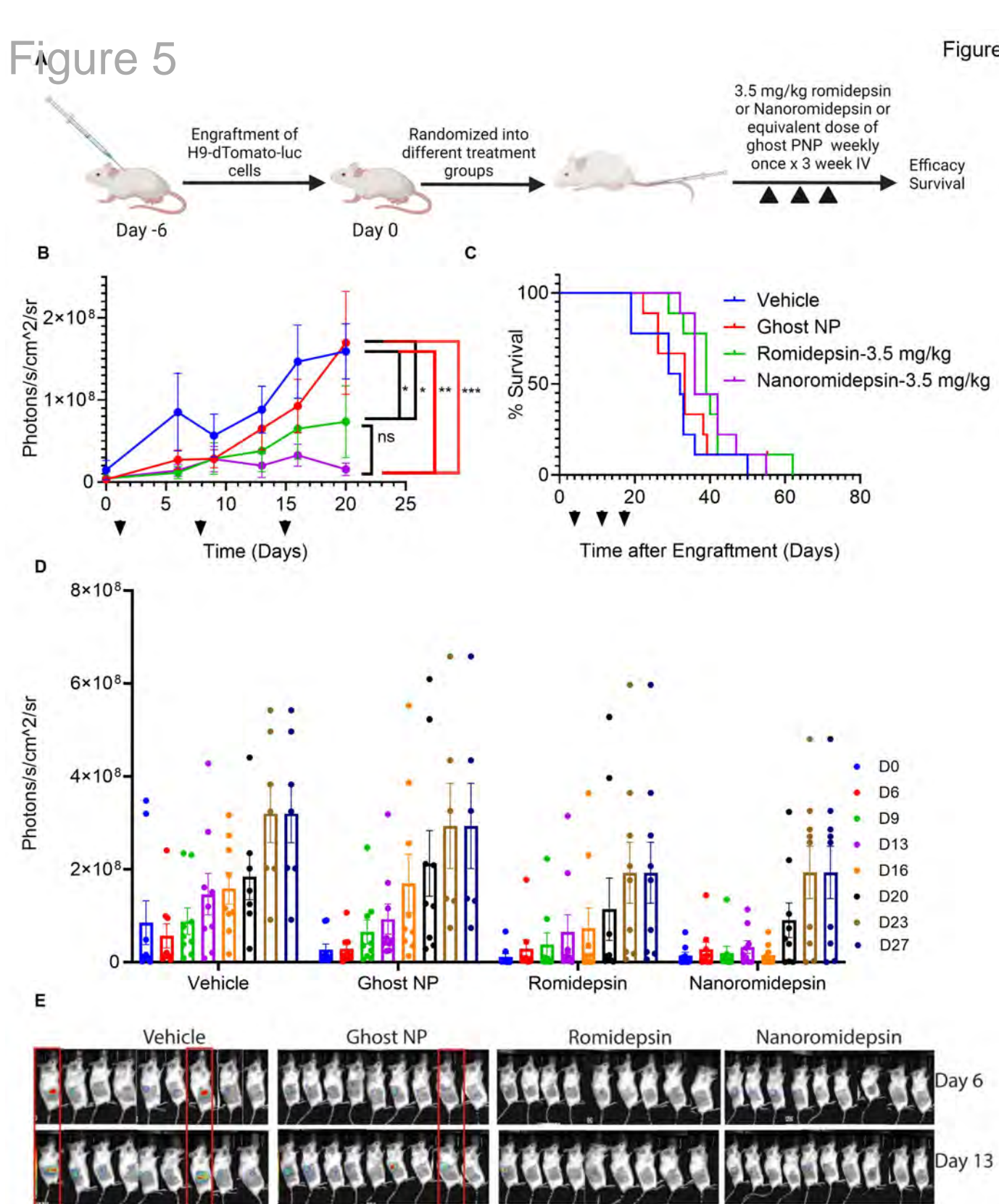






Day 20

Day 27



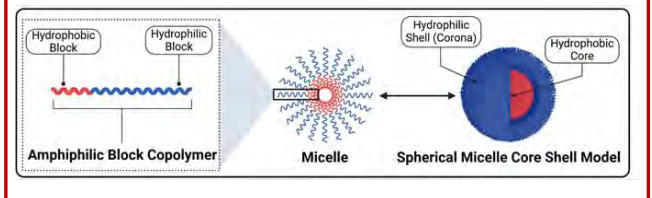
# Development of a Novel Epigenetic Modifier-Based Polymer Nanoparticle and Its Tumor-Killing Effects in T-Cell Lymphoma

### **Context of Research**

- Limited treatment options are available for the treatment of peripheral T cell lymphoma (PTCL).
- Several HDAC inhibitors (HDACi) for PTCL are in regulatory jeopardy, which has created legitimate concerns over future disease management.

#### **Materials and Methods**

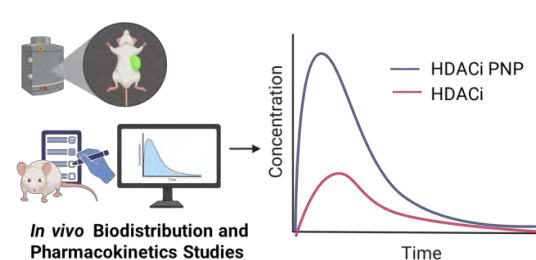
 Synthesis of polymer based HDAC inhibitor nanoparticle using novel nanochemistry platform



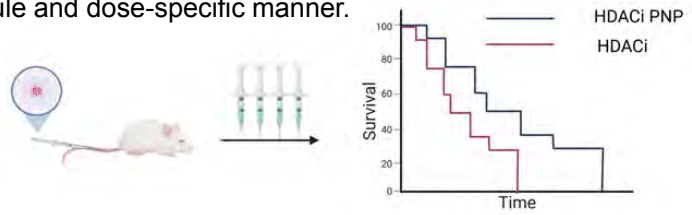
 Pre-clinical development of HDAC inhibitor nanoparticle using in vitro and in vivo murine model

## **Main Findings**

- A unique HDAC inhibitor polymer nanoparticle was developed with higher encapsulation efficiency.
- HDACi polymer nanoparticle showed enhanced pharmacokinetic parameters and bioaccumulation in the tumor compared to the historically approved HDAC inhibitor.



The HDACi polymer nanoparticle demonstrated enhanced efficacy and survival benefits in a T cell lymphoma xenograft mouse model, in a schedule and dose-specific manner.



Conclusions: We have developed a unique, epigenetically targeted, polymeric nanoparticle that has enhanced pharmacokinetics, improved tolerability, and greater efficacy than the historically approved HDAC inhibitor.

Pal et al. DOI: 10.xxxx/blood.2025xxxxxx

